Journal of Sol-Gel Science and Technology
https://doi.org/10.1007/s10971-022-05922-w

ORIGINAL PAPER: SOL-GEL AND HYBRID MATERIALS FOR BIOLOGICAL AND HEALTH (MEDICAL) APPLICATIONS

Antiproliferative effect of 1,10-Phenanthroline coupled to sulfated ZnO nanoparticles in SiHa cervix cancer cell line

Lisbeth Almeida Ramón[1] · Erick N. de la Cruz Hernández[2] · Rosendo López González[1] · María Fernanda Hernández Landero[2] · Patricia Quintana Owen[3] · Cinthia García Mendoza[1] · Getsemani Morales Mendoza[1,4] · Mayra Angélica Alvarez Lemus[1]

Received: 28 April 2022 / Accepted: 1 August 2022

Abstract

During the last decade, nanosized zinc oxide (ZnO) particles have been explored as antiproliferative agents in some cancer cell lines. In this research we propose the surface modification of ZnO with sulfate groups and 1,10-Phenanthroline as antiproliferative agent against SiHa cervical cancer cell line. The ZnO nanoparticles were prepared by two different methods: sol–gel (SG) and precipitation (P). By using sulfate as surface modifier, the anchoring of 1,10-Phenanthroline (Phen) was achieved by wet impregnation. The sol–gel samples showed hexagonal tube-shaped particles of around 100 nm in width, whereas the precipitation method promoted the formation of sphere-like particles with diameters ranging from 20 to 80 nm. The assessment of zeta potential and hydrodynamic size showed the variations due to the surface modifications exhibiting values ranging from −9.9 to −12.4 mV when dispersed in DMEM medium. The in vitro assays revealed the synergistic effect of the modified nanoparticles, which promoted apoptosis and inhibited 65% of cell proliferation in SiHa cell line.

Graphical abstract

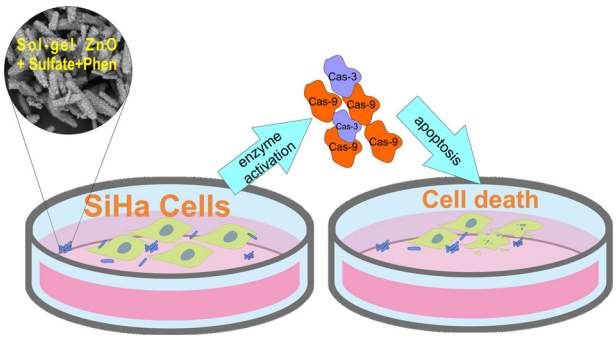

Supplementary information The online version contains supplementary material available at https://doi.org/10.1007/s10971-022-05922-w.

✉ Mayra Angélica Alvarez Lemus
mayra.alvarez@ujat.mx

[1] Laboratorio de Nanotecnología, División Académica de Ingeniería y Arquitectura, Universidad Juárez Autónoma de Tabasco, Km 1 Carr. Cunduacán-Jalpa de Méndez Col. La Esmeralda, C.P. 86690 Cunduacán, TAB, Mexico

[2] Laboratorio de Epigenética y Biología Molecular del Cáncer, División Académica Multidisciplinaria de Comalcalco, Universidad Juárez Autónoma de Tabasco, Ranchería Sur 4a Secc., C.P.86630 Comalcalco, TAB, Mexico

[3] Departamento de Física Aplicada, Centro de Investigación y de Estudios Avanzados del IPN Unidad Mérida, AP 73 Cordemex, C.P. 97310 Mérida, YUC, Mexico

[4] ECOCATAL, Departamento de Química, Universidad Autónoma Metropolitana Iztapalapa, Av. Ferrocarril San Rafael Atlixco, Núm. 186, Col. Leyes de Reforma 1a Secc., C.P. 09310 Ciudad de México, Mexico

Published online: 18 August 2022

Keywords Sulfated ZnO · 1,10-Phenanthroline · SiHa cells · Apoptosis

Highlights

- Wet impregnation allowed to incorporate 1,10-Phenanthroline on the sulfated ZnO nanoparticles.
- The sol–gel and precipitation methods directed to different morphologies affecting the distribution of 1,10-Phenanthroline.
- Sol–gel modified nanoparticles showed 71.5% of apoptosis in SiHa cell line at a dose of 30 μg ml^{-1}.
- The surface modified sol–gel ZnO material activates twice Caspase-9 than the corresponding surface modified ZnO obtained by precipitation method.

1 Introduction

Zinc oxide (ZnO) has been investigated in several biological applications because it exhibits bioactivity against fungi and bacteria, being nanosized ZnO the most promising platform for biomedical uses [1]. Recently, the investigations on bioactive ZnO have been directed toward the treatment of diseases such as cancer, due to its effective cytotoxic activity [2–4]. Like most of the metal oxide-derived nanoparticles, ZnO can be changed through several strategies to improve their properties, and in this sense surface modification represents an excellent strategy for biomedical applications because it turns out in high biocompatibility and/or selectivity toward specific targets [5–7]. The use of an organic compound for this functionalization has been successful not only for modification of the properties of the ZnO, but also for improving the properties of the organic counterparts, for instance: improving solubility, decreasing side effects or toxicity, and maximizing the available surface among others.

In the field of cancer treatment, organometallic compounds had dominated the pharmaceutical industry since the discovery of cisplatin, because a synergistic effect between metal and organic groups provide suitable molecules for the treatment of several types of cancer. Nevertheless, these compounds need to meet the requirements of selectivity, to avoid adverse side effects, and the search of novel compounds that allow less invasive treatments have directed the investigations to broaden the types of materials that can be used for this purpose, particularly oxides such as ZnO, TiO_2 and SiO_2 due to their low costs and relatively non-toxicity.

One of the organic molecules that has been explored for the synthesis of new organometallic drugs is 1,10-Phenanthroline because it exhibits bioactivity against cancer cells when used alone [8–10], nevertheless its lack of selectivity and its capability for disturbing the activity of biological systems has limited its use.

So far, ZnO nanoparticles have been explored in biomedical applications mostly due to its antifungal and bactericidal properties and in the last decade, some studies regarding its cytotoxicity in cancer cells have been published [3]. Cervical cancer is one of the most detected cancers in women according to the World Health Organization, and more than 95% are caused by human papilloma virus. Even though current vaccines help to prevent proliferation of this cancer, when is not diagnosed at early stages, it may spread to other parts of the body increasing the risk of death. As most types of cancers, the treatment for cervical cancer consists of chemotherapy, surgery radiotherapy or a combination of these, with negative impact on the quality of life of patients. These features have encouraged researchers all over the world to look for more efficient treatments, and nanoparticles represent a promising tool to reach both selective and efficient treatments.

The aim of this work was to obtain a conjugated comprised of ZnO + sulfate + 1,10-Phenanthroline by using two sol–gel and precipitation methods, for further evaluation of the effect of their physicochemical properties in their antiproliferative effect on SiHa cervix cancer cells.

2 Experimental

2.1 Chemicals

Zinc (II) acetylacetonate dihydrate ($C_{10}H_{14}O_4Zn$, 97%), sodium carbonate (Na_2CO_3, 98%), zinc nitrate hexahydrate ($Zn(NO_3)_2$, 98%), ammonium persulfate ($(NH_4)_2S_2O_8$) and 1,10-Phenanthroline monohydrate ($C_{12}H_8N_2$ *H_2O, 99%) were purchased from Sigma-Aldrich and used as received. Deionized water (resistivity 18.2 MΩ cm), ethanol (C_2H_5OH, 97%) and ammonium hydroxide (NH_4OH, 28% v/v) were obtained from CIVEQ.

2.2 Synthesis of ZnO nanomaterials

2.2.1 Sol–gel method

In total, 50 ml of an ethanol: water (70:30) mixture were taken and placed into a flask, then the pH was adjusted to 10 with NH_4OH and heated at 70 °C. Later, 2.4 g of zinc

acetylacetonate hydrate were added to this solution. The reaction was kept under stirring for 4 h at 70 °C and aged for 24 h. The resulting gel was filtered (Millipore GTTP) and rinsed alternating ethanol and deionized water thrice. The solvent was evaporated at 70 °C, and the obtained powder was ground in an agate mortar with pestle and calcined at 400 °C during 4 h, 2 °C min^{-1}. After that, the sample was stored and tagged as ZSG.

2.2.2 Precipitation method

In total, 25 ml of 0.25 M Na_2CO_3 were mixed with 25 ml of 0.25 M $ZnNO_3$*$6H_2O$. The pH of the mixture was 10. The solution was left at room temperature and stirred for 24 h until a white precipitate was formed. Then, the suspension was filtered (Millipore GTTP) and rinsed with deionized water thrice. Later, the powder was dried at 70 °C, ground using an agate mortar with pestle and calcined at 400 °C for 4 h, 2 °C min^{-1}. This sample was named as ZP.

2.3 Modification of ZnO particles with sulfate and 1,10-Phenanthroline

Modification of the ZnO surface was performed by impregnation method in two stages, first using ammonium persulfate (S) and later 1,10-Phenanthroline (Phen). In the first stage the ZSG and ZP nanoparticles were sulfated as follows: 1.0 g of nanoparticles (previously dried at 70 °C) were put together with 10 ml of 0.02 M $(NH_4)_2S_2O_8$ and ultrasonicated during 20 min. After that, the mixture was kept under stirring for 24 h, dried at 70 °C and then calcined at 400 °C for 4 h using a rate of 2 °C min^{-1}. Later, the sulfated ZnO nanoparticles were modified using a 5% wt. of Phen solution (dissolved in ethanol), for this purpose 1.0 g of ZnO sulfated nanoparticles and 10 ml of the Phen solution were mixed, and kept under stirring for 24 h, after that the solvent was evaporated at 70 °C in an oven. Finally, the sample was pulverized in an agate mortar with pestle. These samples were labeled as ZSGS-Phen and ZPS-Phen.

2.4 Characterization of the nanomaterials

X-ray diffraction patterns of the samples were obtained in a BRUKER D8 Advance ECO equipment, with Lynx eye detector, Cuα source ($\lambda = 1.5406$ Å), 0.5 s per step and a step size of 0.009°. The patterns were compared to the PDF card JCPDS No. 36-1451 wurtzite-type structure. Fourier transform infrared spectroscopy (FTIR) was performed, and the spectra were collected using a Nicolet FTIR spectrophotometer is50 (Thermo Fisher Scientific). Each sample was measured using ATR module with diamond crystal, from 4000–400 cm^{-1}, and 32 scans. The hydrodynamic size (HS) and zeta potential were measured through dynamic light scattering (DLS) and electrophoretic light scattering respectively. Considering a particle size among 10–100 nm, 10 mg of sample were suspended into 100 ml of dispersant; also considering a particle size among 100 nm to 1 μm, 1 mg of sample was suspended into 100 ml of solvent DMEM/F12 supplemented with 10% FBS medium. Each suspension was sonicated for 30 min. DTS1060C clear-disposable Z and DTS10012 disposable cells were used for zeta potential and particle size measurements, respectively and measured in a ZetaSizer Nanoseries equipment (Malvern Instruments). Morphology of the nanoparticles was characterized by the field emission scanning electron microscope JSM-6010a (JEOL).

2.5 In vitro tests

2.5.1 Cell culture conditions

The SiHa cell line was bought from the ATCC and cultured in DMEM/F12 medium (Invitrogen, life technologies) supplemented with 10% of fetal bovine serum (FBS) (Invitrogen, Life Technologies), penicillin-streptomycin at 37 °C in a humidified 5% CO_2 atmosphere. MTT (cell proliferation kit I) and XTT (cell proliferation kit II) reagents were obtained from Cell Roche®, Sigma-Aldrich

2.5.2 Cell viability assay

Cytotoxicity of the nanoparticles was assessed using primary mononuclear cells, which were isolated from blood samples, using density gradient separation with the reagent Histopaque-1077 (Sigma-Aldrich, USA), according to the instructions provided by the manufacturer. Cells were cultured with RPMI 1640 medium plus 10% of FBS, 10 mM Penicillin-Streptomycin, and 10 mM of L-glutamine (Thermo Fisher Scientific, USA) in a 37 °C, 5% CO_2 humidified incubator. In total, 3×10^3 cells per well were seeded in a 96-well plate (Corning®), and the nanomaterials ZP, ZSG, ZPS-Phen and ZSGS-Phen were incorporated into the medium at a concentration of 10, 20 and 30 μg ml^{-1}. The samples were suspended in saline solution (0.9% NaCl, CS PISA® solution), and sonicated 15 min; control cells were incubated with saline solution only. After 48 h of treatment, the number of viable cells was assessed using MTT assay according with the protocol from the supplier by colorimetric measurement at 550 and 650 nm with an Epoch (Biotek) spectrophotometer. Cytotoxicity of cisplatin (positive control) was evaluated using the same cell culture conditions with XTT assay by colorimetric measurement at 492 and 690 nm with an Epoch (Biotek) spectrophotometer. All assays were performed in triplicate.

2.5.3 Cell proliferation assay

Antiproliferative effect of nanoparticles in SiHa cell line was evaluated using MTT assay. In total, 3×10^3 cells/well were seeded into 96-well microplates (Corning®) with 0.1 ml of complete DMEM/F12 medium supplemented with 10% FBS 24 h before the beginning of the treatment. After 72 h of incubation with 10, 20 and 30 μg ml^{-1} of nanoparticles the medium was aspirated, and cells were washed with PBS. Later, cells were cultured in a mixture of 60 ml of DMEM/F12 medium without FBS plus 40 ml of MTT-solution during 2 h in a humidified incubator (at 37 °C, 5% CO_2). Production of formazan was measured using a microplate reader (Epoch, Biotek) by monitoring the difference in absorbance at 550 and 650 nm. Antiproliferative effect of cisplatin (positive control) in SiHa cell line was estimated using cell proliferation kit II with the same cell culture conditions, and after 72 h of treatment with 10 μM of cisplatin the production of formazan was measured using a microplate reader (Epoch, Biotek) by monitoring the difference in absorbance at 492 and 690 nm. All experiments were repeated three times.

2.5.4 Apoptosis detection by Annexin V-FITC

The Annexin V-FITC apoptosis detection kit was purchased from Invitrogen™ (Thermo Fisher Scientific). In total, 2×10^4 cells were seeded into 24-well plates and were left at 37 °C in a humidified incubator to allow the cells to attach. Then cells were treated with 10 and 30 μg ml^{-1} of ZnO nanoparticles, and a dose at 10 μM of cisplatin was used as a positive control. After 24 h of treatment, cells were harvested, and apoptosis was assessed with Annexin V-FITC apoptosis detection kit according to manufacturer's instruction. Microscopic images were captured using an inverted fluorescence microscope (Zeiss, axiovert A), equipped with an AxioCam ICc3 digital camera.

2.5.5 Western blot

In total, 30 μg of caspase 3 and caspase 9 were dissolved into 10–15% SDS PAGE and transferred to a nitrocellulose membrane. The membrane was subsequently blocked and incubated with corresponding primary antibody at a final dilution of 1:500 for 24 h at 4 °C; horseradish peroxidase-conjugated secondary antibody (Santa Cruz Biotechnology) was added and detected using the ECL kit (Santa Cruz Biotechnology).

2.5.6 Statistical analysis

Statistical significance of the difference between groups was compared by two-way ANOVA with post hoc Tukey's test. p values < 0.05 were considered significant.

3 Results

3.1 Characterization of ZnO-based nanomaterials

To know the specific area of both ZnO raw materials (ZSG and ZP), N_2 physisorption isotherms were obtained and Brunauer-Emmet-Teller (BET) specific area value for each sample was estimated. As it has been widely reported, ZnO-based materials are characterized by possessing low area, for the samples here reported these values were 5 and 31 $m^2 g^{-1}$, for ZSG and ZP respectively, where the effect of the synthesis method clearly affected this parameter. An important effect due to sulfatation was observed for the ZP sample which specific surface area BET decreased to 4 m^2/g (Fig. S1, ESM_1).

Nevertheless, both methods of synthesis directed to the formation of cubic crystalline wurtzite-type structure of ZnO (Fig. 1), where it can be observed that the sulfatation of the samples did not affect neither crystalline phase nor crystallite size, as can be inferred from the width of the characteristic peaks attributed to wurtzite. But the incorporation of the organic molecule 1,10-Phen, can be inferred from the presence of small peaks observed below 30°(2θ) in both ZSGS-Phen and ZPS-Phen diffractograms, being clearer for the sol–gel-based sample. Figure 1b displays a magnification of the 12–30° (2θ) region for each of the diffractograms for ZSGS-Phen and ZPS-Phen samples together with the XRD pattern of 1,10-Phenanthroline (Full spectrum can be consulted in Fig. S2, ESM_1), where the signals around 15.16°, 17.2°, 19.9°, 26.4° and 27.2° (2θ) correspond to peaks observed in the Phen sample. The crystallite size was estimated by the Scherrer equation from the (101) reflection plane for all the samples (insert in Fig. 1a), where the smallest sizes were exhibited by both pristine samples.

The IR spectra for all the samples were collected and are displayed in Fig. 2. In the mid-infrared region, bands below 600 cm^{-1} have been reported for Zn-O stretching vibrations, and their location depends on the synthesis method, precursors, particle size, and even crystalline structure [11–13]. In this research, we observed some differences in the band located between 400–600 cm^{-1} for ZnO pristine samples (Fig. 2a, b). The spectrum for ZSG material exhibited a characteristic band centered at 402 cm^{-1} with a shoulder around 455 cm^{-1}, while these bands were located at 417 and 464 cm^{-1} for the ZP material. These differences can be attributed to the method of synthesis that certainly affected shape and size of the particles. In the high energy region of the spectra, we observed the bands that corresponds to O-H stretching vibrations between 3750–3000 cm^{-1}, which are often associated to the surface hydroxyl groups commonly present in metal oxides. Since modification of ZnO surface was performed, a magnification of the

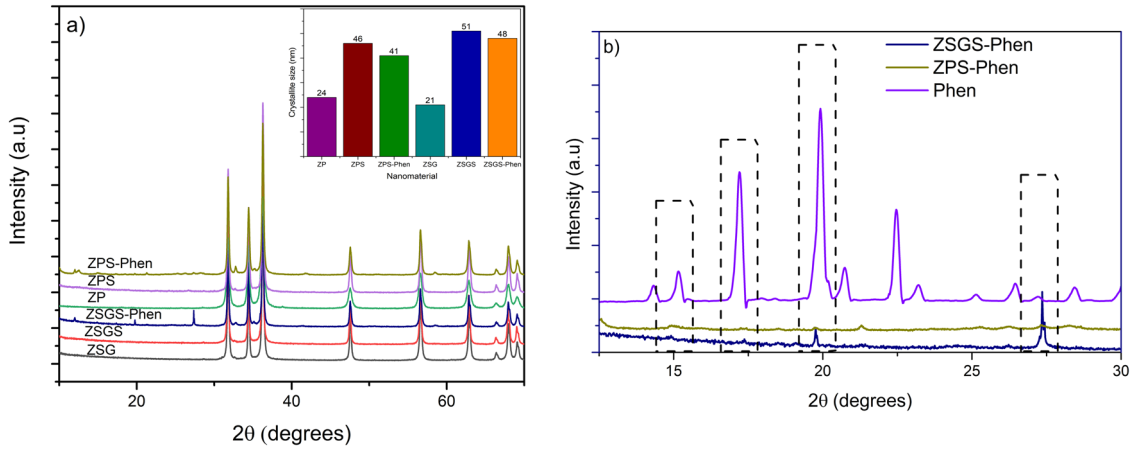

Fig. 1 X-ray diffraction patterns of **a** unmodified ZnO samples, sulfated samples and sulfated samples coupled to 1,10-Phenanthroline. The insert corresponds to XRD pattern of 1,10-Phenanthroline, and **b** magnification of the 12–30°(2θ) region for ZSGS-Phen, ZPS-Phen and Phen (1,10-Phenanthroline) samples

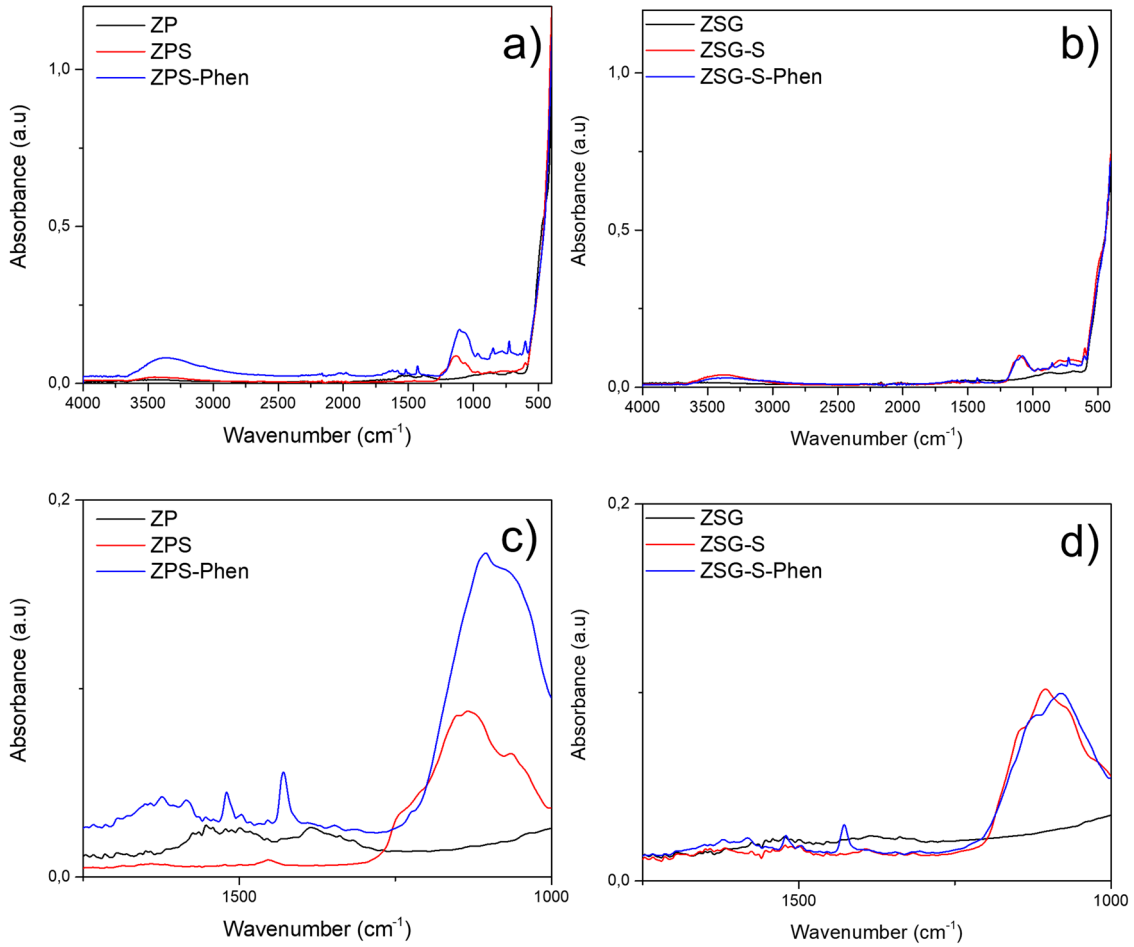

Fig. 2 Infrared spectra of pristine ZnO, sulfated-ZnO and sulfated-ZnO with phenanthroline samples. The mid-IR spectra of **a** precipitation and **b** sol–gel obtained samples calcined at 400 °C. Amplification of the mid-energy region for **c** precipitation and **d** sol–gel samples

1750–1000 cm^{-1} zone is displayed in Fig. 2c, d. First, the sulfate addition can be confirmed due to the presence of a low intense broad band between 1300–1000 cm^{-1} region. For both sulfated samples, the corresponding ZPS and ZSGS spectra showed a band attributed to stretching vibration from S-O, which are centered at 1183 cm^{-1} for

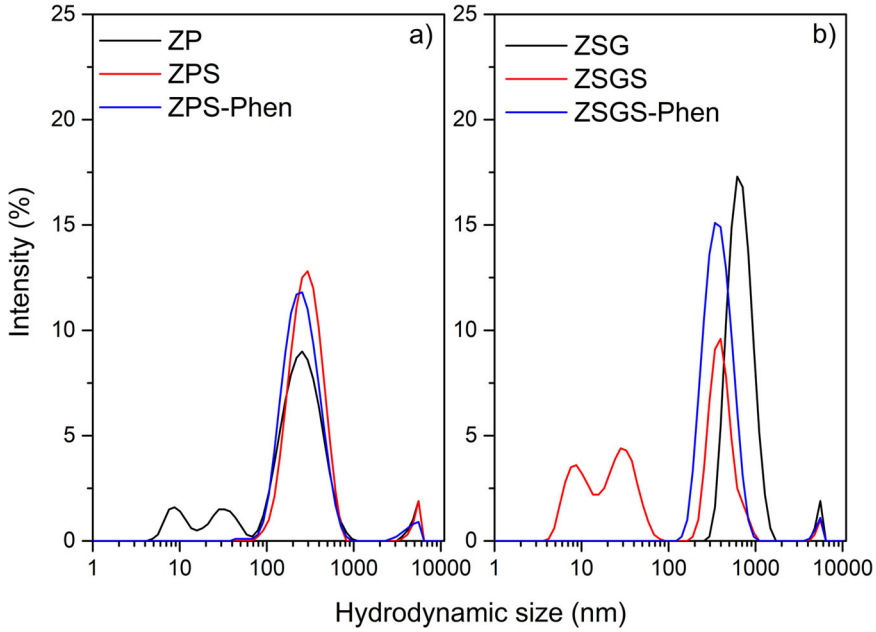

Fig. 3 Particle size distribution of the nanoparticles measured by DLS and dispersed in DMEM medium at 25 °C. **a** ZnO samples from precipitation method and **b** corresponds to sol–gel derived materials

Table 1 Hydrodynamic size and zeta potential measurements of the ZnO nanomaterials, using DMEM (Dulbecco's Modified Eagle Medium) as dispersant

Sample ID	Zeta potential (mV)	Z_{avg} (nm)	PDI
ZP	−9.9	151	0.592
ZPS	−9.8	252	0.493
ZPS-Phen	−12.4	272	0.378
ZSG	−11.9	706	0.445
ZSGS	−9.1	96	0.336
ZSGS-Phen	−12.4	354	0.297

Each value represents the average of three measurements

ZPS and at 1160 cm^{-1} for ZSGS. The frequency of the vibrations corresponding to free sulfate groups can be assigned to the bands centered at 1054 and 960 cm^{-1} for ZPS and 1072 and 966 cm^{-1} for ZSGS [14]. When phenanthroline impregnation was performed, the location of these bands was shifted toward lower wavenumbers and appear overlapped with the signals of C-H stretching vibration from the phenanthroline ring at 725 and 854 cm^{-1}. However, the bands corresponding to C-N bond vibrations are clearly observed around 1428 and 1520 cm^{-1}, finally the band corresponding to the vibrations of the ring from free phenanthroline was identified around 1584 cm^{-1} [15].

Since the present work aims the use of ZnO nanoparticles in biological medium, we determined the size and zeta potential of the obtained nanomaterials using cell culture medium DMEM/F12 supplemented with 10% FBS. The data and distributions of HS for all the samples are shown in Fig. 3 and Table 1. We observed that the average size measured by DLS technique for ZP dispersed in DMEM was 151 nm while the average size for ZSG reached 706 nm (Table 1). Regarding zeta potential measurements, the values of this parameter were all close to each other, and electronegative in all cases, but when the ZP sample was sulfated, the zeta potential value was slightly higher than that observed for sol–gel sulfated sample ZSGS. When Phen was incorporated in the surface of the ZnO-based nanomaterials this parameter was the same in both cases.

Regarding the morphology of the as-synthesized nanomaterials, we have previously reported on the effect of zinc precursor in the shape of ZnO nanoparticles which directs to the formation of tubular hexagonal shaped particles, in comparison with previously reported by our group when no additives are used for adjusting pH, the dimensions of the walls varied, being thicker than those obtained under alkaline conditions [16]. Moreover, the formation of ZnO hollow nanoparticles is originated from preferential dissolution inside of ZnO rods and extraction of Zn^{2+} along axis c [17]. From Fig. 4, we concluded that the nanomaterial obtained by the sol–gel method (Fig. 4a) exhibited large particles whereas precipitation synthesis promoted the obtaining of smaller semi-spherical agglomerated particles with sizes ranging from 10 to 50 nm in length (Fig. 4b). The incorporation of sulfate affected the surface of the ZSG particles, as they appear lower in size and apparently less smoothed than bare ZnO obtained by sol–gel (Fig. 4b), whereas ZPS particles increased in size (Fig. 4e). Finally, when 1,10-Phenanthroline was incorporated on the sulfated particles (Fig. 4c, f) can be clearly noticed that for the sol–gel sample small particles of around 50 nm are distributed over the surface of the ZSGS nanoparticles; this feature was not observed in ZP particles, however from the

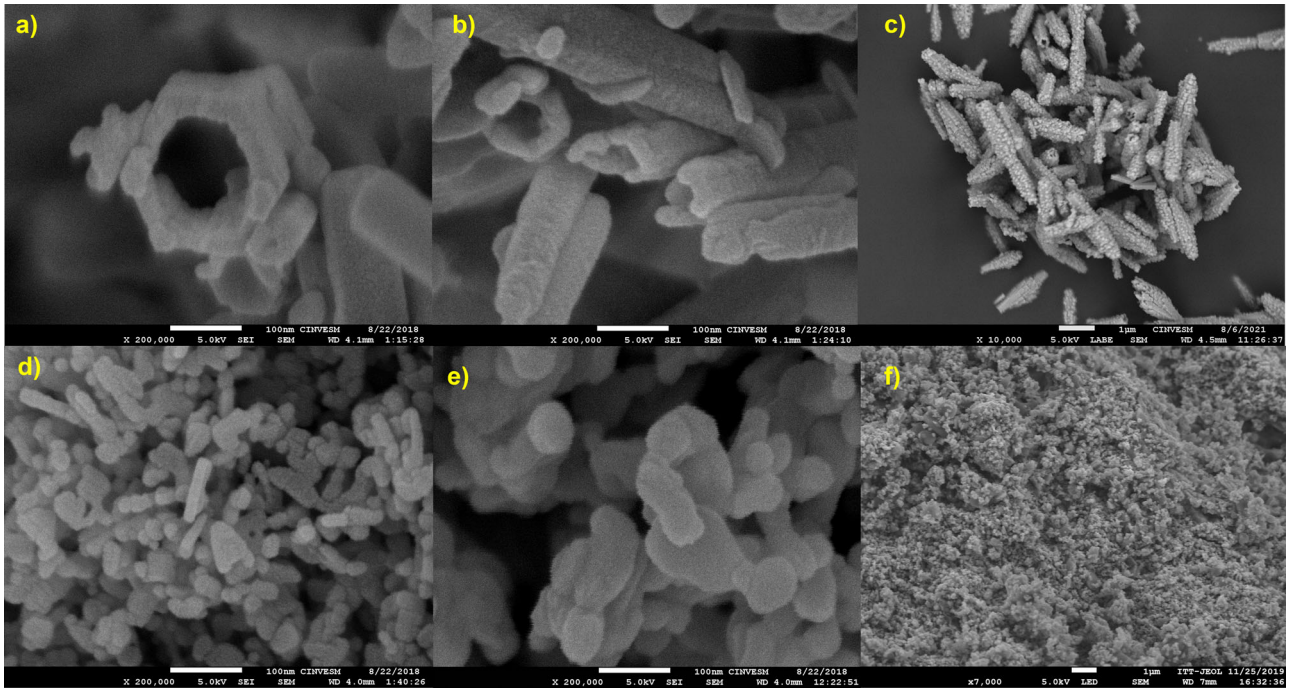

Fig. 4 FESEM micrographs of nanoparticles **a** ZSG, **b** ZSGS, **c** ZSGS-Phen, **d** ZP, **e** ZPS and **f** ZPGS-Phen

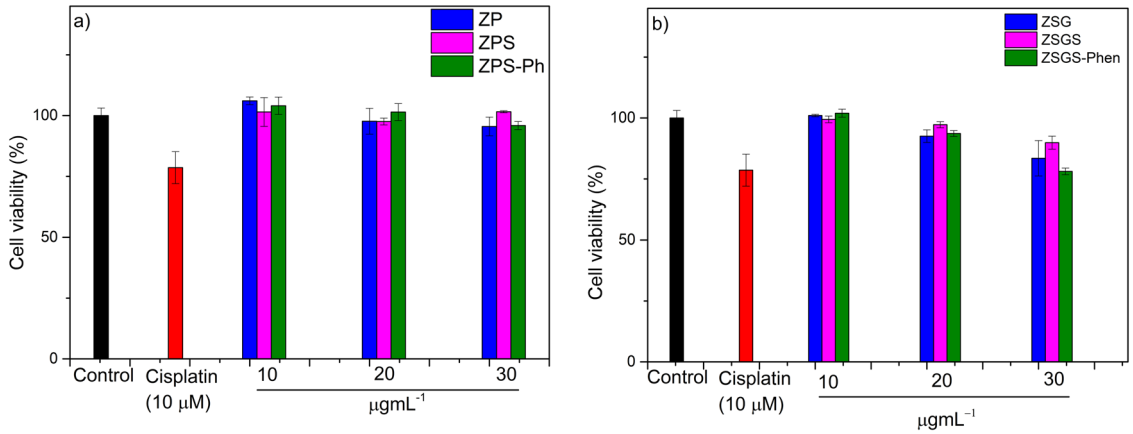

Fig. 5 Cell viability by MTT technique of monocytes isolated from the peripheral blood after 48 h incubation with 10, 20 and 30 μg ml^{-1} of **a** ZnO samples obtained by precipitation and **b** ZnO samples obtained by sol–gel. A 10 μM cisplatin solution was used as positive control. Bars indicate the standard deviation of the three measurements

microphotography we can assume that the two added components increased the size of the particles.

3.2 In vitro assays

The results from the cell viability assay using human monocytes after 48 h with 10, 20 and 30 μg ml^{-1} of each material are shown in Fig. 5. We observed that all nanoparticles showed no effect in cell viability at a dose of 10 μg ml^{-1}, but when the dose is increased to 20 μg ml^{-1}, for the sol–gel based materials the cell viability was affected decreasing in about 8%, when comparing to ZP at the same dose the cell viability decreased only in 2%, which can be considered as no significant, assuming that ZP and ZPS-Phen are nearly non-toxic to peripheral cells. In general, toxicity of nanoparticles is dose-dependent, nevertheless the type of nanoparticle and its properties define the limits of toxic doses [18]. Under the experimental conditions here reported, at a dose of 30 μg ml^{-1} of ZSG and ZSGS-Phen, it can be observed that cell viability decreased up to 90 and 83%, and again ZP and ZPS-Phen nanoparticles showed lower toxicity than sol–gel materials, since cell viability was kept at 96%. Regarding sulfated samples ZPS a slight decrease in cell viability at the dose of 20 μg ml^{-1} was

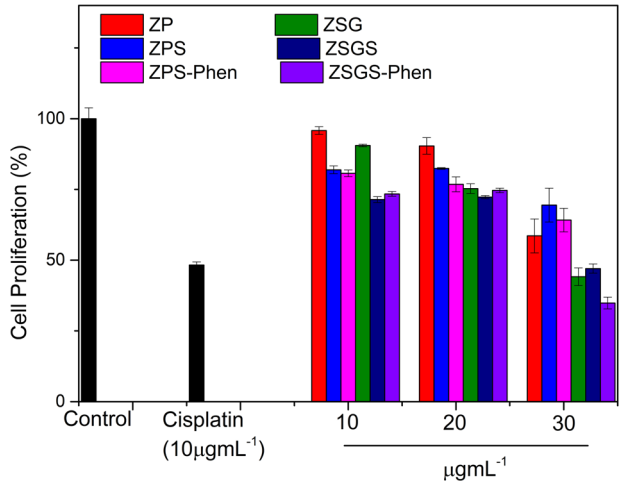

Fig. 6 Cell proliferation by MTT technique of SiHa cell line after 72 h of incubation with 10, 20 and 30 μg ml^{-1} of ZP, ZPS, ZPS-Phen, ZSG, ZSGS and ZSGS-Phen materials. A 10 μM cisplatin solution was used as positive control

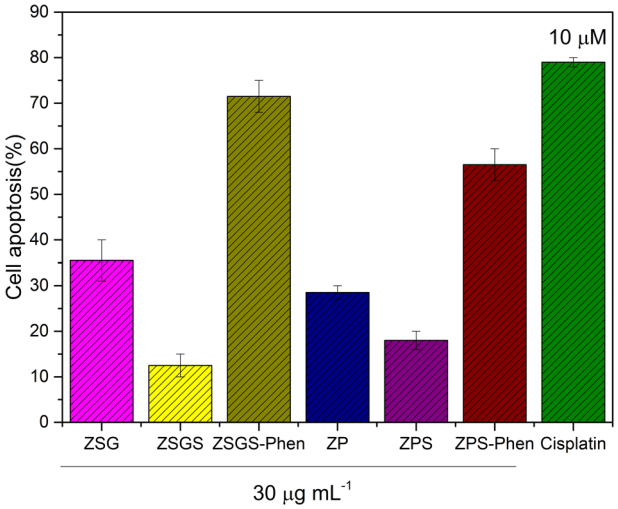

Fig. 7 Cell apoptosis by Annexin V-FITC after 24 h of incubation with 10 and 30 μg ml^{-1} of ZSG, ZSGS-Phen, ZP and ZPS-Phen materials. A 10 μM cisplatin solution was used as positive control

observed, nevertheless it was very close to that observed for the unmodified ZP nanoparticles. On the other hand, the sol–gel sulfated sample ZSGS exhibited a dose-dependent behavior, but with less toxic effect than non-sulfated sample ZSG. As a positive control, the results from exposure of cells to cisplatin (10 μM) are included, being clear the negative effect of this compound in the cells, which reached 80% of viable cells.

As part of the objectives of this work, the capability of functionalized ZnO nanoparticles as antiproliferative agents in SiHa cervix cancer cells was evaluated. After incubation of SiHa cells with the distinct ZnO nanoparticles the cell proliferation percentages were calculated, and the results are shown in Fig. 6. The differences in the antiproliferative activity observed for the ZnO samples can be related to the physical-chemical properties provided by the synthesis route. The most effective concentration for the treatment of ZnO nanoparticles was 30 μg ml^{-1} and the material that showed the highest effect on the inhibition of cell proliferation was ZSGS-Phen. Regarding the ZnO obtained by precipitation method, for pristine ZnO (ZP) material at doses below 30 μg ml^{-1} showed no significant effect in cell proliferation, and a slight effect was observed for ZPS-Phen nanoparticles at doses of 10 and 20 μg ml^{-1} where proliferation was inhibited in 19% and 23%, respectively. This inhibition reached 36% when 30 μg ml^{-1} dose was administered, but this result was slightly higher than the obtained for ZP nanoparticles without modification at the same dose.

The treatment of the cancer cells with ZnO nanoparticles obtained by the sol–gel methodology caused scant inhibition at the lower dose, decreasing in 9% and 27% with ZSG and ZSGS-Phen, respectively. By increasing the concentration of nanoparticles up to 20 μg ml^{-1}, the cell proliferation was the same for both samples (around 26%), from these results we noticed a similar behavior between both experiments, since at doses of 10 and 20 μg ml^{-1} functionalized samples the antiproliferative effect seems to remain almost the same, and it was at the higher dose that the differences between the effect of both types of samples became clearer. It is worth to mention that both sulfated samples ZPS and ZSGS, showed a similar trend when 10 and 20 μg ml^{-1} of each nanomaterial were used, since the effect in SiHa cells was very close to the ZP and ZSG nanomaterials, respectively.

Evaluation of the percentage of apoptosis induced in SiHa cells after the treatment with nanoparticles was performed using Annexin V-FITC and we observed that the antiproliferative effect in the cervical cancer cell line was mainly due to apoptosis of the cells. In Fig. 7, it can be observed that bare ZnO materials induced apoptosis, but sol–gel ZnO induced slightly more than the observed for ZnO obtained by precipitation method. When sulfatation of the ZnO is achieved, there is a clear and significant difference when compared to ZnO alone, observing that cells treated with ZSGS has lower apoptosis percentage than ZPS sample. Finally, when phenanthroline is present in the samples, the difference between both samples was significant, since ZSGS-Phen induced 71.5% of apoptosis whereas ZPS-Phen reached 56.5%. As positive control, the test was also performed for the cells treated with 10 μM cisplatin solution, which caused 79% of apoptosis in the treated cells.

The expression of caspases 3 and 9, two proteins involved in apoptotic route was determined and the results are shown in Fig. 8. The activation of this family of proteins takes place when the cell is about to die by apoptosis, and

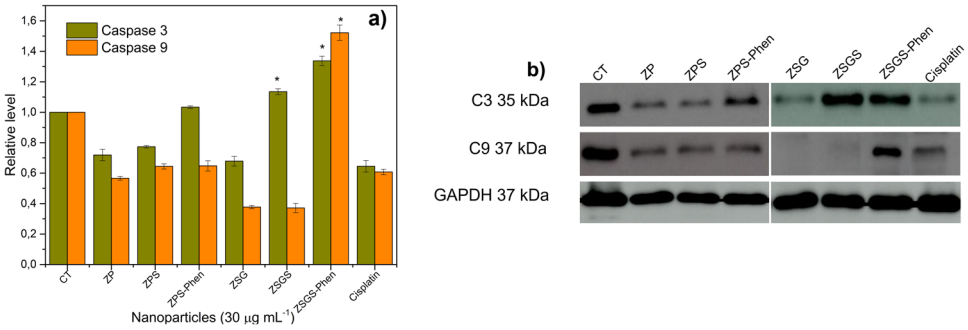

Fig. 8 **a** Relative quantity of the expression of caspase-3 and caspase-9 from the cell incubated with the different cells, at the dose of 30 μg ml^{-1}, **b** expression of the enzymes obtained by Western blot. The figure shows the corresponding levels of GAPDH as loading controls. CT control, $*p < 0.05$

each one of them has a distinct role in the cell death process. From our results, we observed that for all the six different ZNO-based materials caspase-3 expression was higher than caspase 9 except for the ZSGS-Phen sample which promoted higher expression of caspase 9 than the observed for caspase 3. It can be noticed that ZSGS sample promoted a relatively high expression of caspase 3 when compared to cisplatin treatment. Considering both ZPS-Phen and ZSGS-Phen modified samples, the sol–gel sample induced the highest activation of caspase 9 when compared to the rest of the samples, moreover the activation of caspase 3 was like caspase 9, which can indicate a regulated ratio between both enzymes allowing the cell to die by an intrinsic pathway more efficiently than the observed for the other particles that ZSGS-Phen nanomaterial activated the expression of caspase 9 almost threefold the expression of caspase 3, and with a higher relative quantity than the positive control cisplatin.

4 Discussion

The surface modification of nanoparticles, has attracted interest and relevance due to the enhancement of its biological activity, ammine, sulfate and hydroxyl functional groups are among the most common modifications reported for biological applications. Regarding sulfatation of metal oxide nanoparticles, it has been extensively reported for instance, that this modification induces acidity on the metal oxide surface due to the incorporation of sulfate ions on the surface of the oxide [19], which provides more reactivity to the material. With this idea in mind, we modified the surface of ZnO for further coupling with 1,10-Phenanthroline, a molecule with very attactive properties such as basicity, aromaticity, strong chelating activity [20], and a well known biological activity due to the easily intercalation with DNA base pairs that make it suitable in the development of anticancer drugs [21].

The confirmation of the presence of both sulfate species and Phen was performed by powder XRD and FTIR analyses. From the XRD pattern, we observed the presence of peaks attributed to 1,10-Phenanthroline, which main characteristic peak appears around 20° (2θ) [22]. Although not all the corresponding signs for Phen can be observed, the appearance of new features in the ZnO pattern can be attributed to interactions with the surface modifiers.

Wet impregnation is a practical method for allocation of molecules on the surface of inorganic oxides [23], according to our results and considering that the samples were rinsed prior to calcination, we assume from the FTIR spectra that sulfate and phenanthroline molecules were attached to the surface of ZnO nanoparticles, observing no differences related to the process of synthesis. The bands observed in the 1250–900 cm^{-1} in the spectra of the sulfated samples are very close to those reported by Istadi et al. [24]. Undoubtely, the observations made by infrared spectroscopy are not conclusive, but it allowed us to infer the interactions among the three components conforming the samples, i.e., ZnO-sulfate-Phen.

The surface composition of the nanoparticle will determine the strength and the capacity to adsorb biomolecules, modifying not only the surface electrical charge of nanoparticles but also their aggregation.

By performing the measurements of HS, we noticed that ZSG particles are larger than ZP which is attributed mainly to the precursor, since it has been reported the obtaining of larger particles when acetylacetonate is used as source of zinc [16]. By observing the microphotographs of functionalized samples (ZSGS-Phen and ZPS-Phen), it is very clear the formation of smaller particles on the surface of ZnO hexagonal tubes, which we assume are comprised of phenanthroline molecules and sulfate groups. This can be attributed to the fact that for the sol–gel sample, the tubular structure is formed with very low porosity, and the sulfate ions are only deposited on the surface and further anchorage of the phenanthroline organic molecules takes place forming small aggregates instead of a well dispersed layer, as it has been reported for carbon nanotubes where supramolecular π-π stacking occurs [25], but once the first molecules are on the surface of the sample, the interactions between aromatic rings of the subsequently adsorbed molecules can take place by preferential T-shaped or parallel displaced

geometry leading to the formation of the observed aggregates [26]. Two particular changes were observed regarding the size distribution curves showed in Fig. 3, the first one is related to the disappearance of the two signals at sizes below 100 nm for the ZP sample; since SEM images showed the presence of small quasi-spherical particles, we assume that when sulfatation of the ZP sample occurs the presence of different species derived from sulfate groups, can lead to the formation of larger particles after calcination. On the contrary, for the ZSG sulfated sample the appearance of signals indicating the presence of particles with sizes below 100 nm can be related to what was observed in SEM images, where the appearance of small spherical-shaped particles around the hexagonal tubular sol–gel ZnO particles was noticed, and some of these particles can be loosely attached to the surface that when suspended in DMEM, are detached and contribute to the appearance of those signals. In the other hand, the ZPS-Phen presented no changes in the shape of its particles but in the size, being less uniform and larger than those obtained for ZP sample. It is worth to notice the fact that after sulfatation, the specific area of the ZP sample decreases which may indicate the coverage of the pores by the sulfate groups, and by considering that from SEM images of the ZPS-Phen sample probably the smaller particles are formed mainly of Phen due to the small size of the ZP particles. From these observations and considering the presence of functional groups from sulfate and phenanthroline detected by FTIR spectroscopy in both functionalized samples, it can be assumed that for ZPS-Phen sample attachment of sulfate and phenanthroline on the surface of ZnO particles took place in a more suitable way, allowing better dispersion of the organic molecule. The differences between particle size and HS measured by DLS relays in the ability of nanoparticles to adsorb molecules, such as proteins which are present in biological media [27].

On the other hand, zeta potential is one of the most important characteristics that influences the interactions between nanoparticles and biomolecules [28, 29]. ZnO materials here reported, exhibited similar zeta potential values, observing that there was no significant difference between the two methods of synthesis, being the precipitation sample (ZP) the one with the slightly lowest value. Meißner et al. reported on the zeta potential for ZnO hydrophilic coated particles measured in DMEM, and then compared with ZnO lipophilic particles observing an increase on the zeta value for lipophilic covered nanoparticles [30], in our work the incorporation of 1,10-Phenanthroline lead to a slight increase in the electronegative zeta potential of ZnO particles, which can be interpreted as the effect of 1,10-Phenanthroline, since this molecule is considered as a lipophilic chelator [31]. Similar behavior has been reported for some silica nanoparticles [32], and in general it has been reported that when measured in DMEM metal oxide nanoparticles they exhibit negative zeta potential values ranging from around −25 to −5 mV [33].

Several groups have reported on the possible mechanisms by which ZnO interacts with cells, and bacteria inducing cell death. Among them, release of zinc ions and formation of reactive oxygen species (ROS) are the most confirmed, although the small size also plays an important role on internalization and thus later interactions between cell organelles and nanoparticles [34]. Although ZSGS-Phen did not exhibit the lowest hydrodynamic and particle size, this nanomaterial showed the major activity against cell proliferation in SiHa cells. We propose that the presence of the clusters of sulfates-phenanthroline distributed on the surface of the particles could be acting as active sites that interact with SiHa cells through the cell membrane.

Caspases play an important role in cell signaling for apoptosis (programmed cell death), these are a type of specific proteases. Among these, the so-called apoptotic caspases (involved in cell death by apoptosis) can be subdivided into two groups: initiators (caspases 2, 8, 9 and 10) and executioners (caspases 3, 6 and 7). Caspase 9 is associated to the intracellular pathway called intrinsic pathway, which usually is the route used by cells as a response to stress that can be derived from DNA damage of ROS generation [35]. This enzyme promotes caspase 3 activation, and it is related to the formation of ROS during apoptosis mechanism, whereas caspase-3 is responsible for limiting ROS production [36]. For the ZSGS-Phen sample, we observed that the relative level of expression for both enzymes was the highest and From the observed results on the expression of these two enzymes, we noticed that ZSGS-Phen sample was the one with the highest expression of caspase 9, this effect has been also reported for ZnO-based nanoparticles for oral squamous cell carcinoma [37], and human multiple myeloma [38] where disruption of mitochondria membrane potential occurs. Thus, it can be assumed that the interaction between cells and ZnSGS-Phen nanomaterial activates faster the cascade of apoptosis via ROS production.

It has been reported that SiHa cell line overexpress E6 and E7 oncoprotein which are present on human papilloma virus and contains amino and carboxyl groups bond with zinc [39], this could explain their affinity to treatments with ZnO nanoparticles. A few studies on the cytotoxic effect of ZnO nanoparticles have been performed on human papilloma cells, for instance Mohamed Asik et al. reported on the activity of biogenic ZnO nanoparticles in SiHa, and they found that after the treatment with nanoparticles 75% of the cells suffered apoptosis at a dose of 35 μg ml^{-1} but Annexin V analysis showed also a significant necrotic percentage [40]. On the other hand, a study on HeLa cells revealed that ZnO inhibited the cell viability significatively above

concentrations of 40 µg ml^{-1} [41], while for Human gastric and melanoma cancer cells, Ag-ZnO composites have also demonstrated significant effect [40]. With our result, we demonstrated the potential of sulfatation as a strategy for incorporating 1,10-Phenanthroline, a bioactive molecule with a strong potential as anticancer agent when combined with phenanthroline derivatives on the surface of ZnO particles for improving the antiproliferative effect of ZnO by means of the apoptotic route [42–44].

5 Conclusions

The obtained shape and size of ZnO nanoparticles are strongly associated to the synthesis method, zinc precursor, solvent and the thermal treatment, these parameters influence the arrangement of the atoms during the first stages of the synthesis of ZnO nanoparticles. One of the most important achievements in this work was the functionalization of the ZnO nanomaterials, the use of sulfate allowed the anchoring of the organic molecule 1,10-Phenanthroline, which is of biological interest due to its chemical properties. Despite the apparent disadvantage created in the HS of the particles by using the biological medium (DMEM), this did not limit the bioactivity of the particles, and further analysis related to the full mechanism will be needed.

The most interesting feature observed for in vitro assays was the different behavior observed in the antiproliferative effect, which obeys the physical-chemical properties provided by parameters and conditions of synthesis method. SiHa cell line was sensitive to the dose of 30 µg ml^{-1} of each nanoparticle, the ZSGS-Phen material exhibited the higher antiproliferative effect (65%) promoting the activation of caspase 9 more than caspase 3. Here, we demonstrated that 1,10-Phenanthroline was successfully attached to the surface of the ZnO nanoparticles and its biological activity was preserved, improving the cytotoxicity of bare ZnO, which opens the door for further investigations in this area.

Acknowledgements The authors would like to thank to the UJAT and LANNBIO-CINVESTAV Mérida for the facilities and projects INFRA-269701, INFRA-269784, FOMIX Yucatán 2008-108160, CONACYT LAB-2009-01-123913, 294643, 188345 and 204822. LAR acknowledge to CONACYT for the doctoral scholarship.

Author contributions All authors contributed to the study conception and design. Material preparation, data collection and analysis were performed by LAR, ENCH, GMM and MFHL. The first draft of the manuscript was written by LAR, RLG and CGM, all authors commented on previous versions of the manuscript and the submitted version was revised by PQO and MAAL. All authors read and approved the final manuscript.

Funding The Doctoral scholarship for LAR was provided by CONACYT-Mexico and the projects acknowledged in the Acknowledgement section correspond to the acquisition of equipment for the laboratories where the investigation was performed.

Compliance with ethical standards

Conflict of interest The authors declare no competing interests.

References

1. Siddiqi KS, Ur Rahman A, Tajuddin, Husen A (2018) Properties of zinc oxide nanoparticles and their activity against microbes. Nanoscale Res Lett 13:141. https://doi.org/10.1186/s11671-018-2532-3
2. Tianke Z, Du E, Liu Y, Cheng J, Zhang Z, Xu Y, Qi S, Chen Y (2020) Anticancer effects of zinc oxide nanoparticles through altering the methylation status of histone on bladder cancer cells. Int J Nanomed 15:1457–1468. https://doi.org/10.2147/IJN.S228839
3. Wiesmann N, Tremel W, Brieger J (2020) Zinc oxide nanoparticles for therapeutic purposes in cancer medicine. J Mater Chem B 8:4973–4989. https://doi.org/10.1039/D0TB00739K
4. Anjum S, Hashim M, Malik SA, Khan M, Lorenzo JM, Abbasi BH, Hano C (2021) Recent advances in zinc oxide nanoparticles (ZnO NPs) for cancer diagnosis, target drug delivery, and treatment. Cancers 13:4570. https://doi.org/10.3390/cancers13184570
5. Saffar MA, Eshaghi A, Dehnavi MR (2022) Superhydrophobic ZnO thin film modified by stearic acid on copper substrate for corrosion and fouling protections. J Sol-Gel Sci Technol 101:672–682. https://doi.org/10.1007/s10971-022-05749-5
6. Yang Z, Ye Z, Zhao B, Zong X, Wong P (2010) Synthesis of ZnO nanobundles via sol–gel route and application to glucose biosensor. J Sol-Gel Sci Technol 54:282–285. https://doi.org/10.1007/s10971-010-2191-z
7. Giridhar M, Bhojya Naik HS, Sudhamani CN, Kenchappa R, Patil S (2019) Antibacterial activity of water-soluble dye capped zinc oxide nanoparticles synthesised from waste Zn–C battery. SN Appl Sci 1:297. https://doi.org/10.1007/s42452-019-0272-3
8. Kumar M, Uday Parsekar S, Duraipandy N, Syamala Kiran M, Koley AP (2019) Synthesys, DNA binding and in vitro cytotoxicity studies of a mononuclear copper (II) complex containing N2S(thiolate)Cu core and 1,10-phenanthroline as a coligand. Inorg Chim Acta 484:219–226. https://doi.org/10.1016/j.ica.2018.09.044
9. Đurić SŽ, Mojicevic M, Vojnovic S, Wadepohl H, Andrejević TP, Stevanović NL, Nikodinovic-Runic J, Djuran MI, Glišić BĐ (2020) Silver(I) complexes with 1,10-phenanthroline-based ligands: the influence of epoxide function on the complex structure and biological activity. Inorg Chim Acta 502:119357. https://doi.org/10.1016/j.ica.2019.119357
10. Nunes P, Correia I, Cavaco I, Marquez F, Pinheiro T, Avecilla F, Costa Pessoa J (2021) Therapeutic potential of vanadium complexes with 1,10-phenanthroline ligands, quo vadis? Fate of complexes in cell media and cancer cells. J Inorg Biochem 217:111350. https://doi.org/10.1016/j.jinorgbio.2020.111350
11. Soli J, Kachbouri S, Elaloui E, Charnay C (2021) Role of surfactant type on morphological, textural, optical, and photocatalytic properties of ZnO nanoparticles obtained by modified sol–gel. J Sol-Gel Sci Technol 100:271–285. https://doi.org/10.1007/s10971-021-05653-4
12. Sowri Babu K, Ramachandra Reddy A, Sujatha CH, Venugopal Reddy K, Mallika AN (2016) Synthesis and optical characterization of porous ZnO. J Adv Ceram 2:260–265. https://doi.org/10.1007/s40145-013-0069-6

13. Hosono E, Fujihara S, Kimura T, Imai H (2004) Non-basic solution routes to prepare ZnO nanoparticles. J Sol-Gel Sci Technol 29:71–79. https://doi.org/10.1023/B:JSST.0000023008.14883.1e
14. Zhong J, Li J, Zeng J, Huang S, Hu W (2014) Enhanced photocatalytic activity of sulfated silica-titania composites prepared by impregnation using ammonium persulfate solution. Mater Sci Semicond Process 26:62–68. https://doi.org/10.1016/j.mssp.2014.04.008
15. Sadeek SA, El-Hamid SMA (2016) Preparation, characterization and cytotoxicity studies of some transition metal complexes with ofloxacin and 1,10-phenanthroline mixed ligand. J Mol Struct 1122(3):175–185. https://doi.org/10.1016/j.molstruc.2016.05.101
16. Uribe-López M, Hidalgo-López MC, López-González R, Frías-Márquez DM, Núñez-Nogueira G, Hernández-Castillo D, Alvarez Lemus MA (2021) Photocatalytic activity of ZnO nanoparticles and the role of the synthesis method on their physical and chemical properties. J Photochem Photobio A Chem 404:112866. https://doi.org/10.1016/j.jphotochem.2020.112866
17. Wang H, Li M, Jia L, Li L, Wang G, Zhang Y, Li G (2010) Surfactant-assisted in situ chemical etching for the general synthesis of ZnO nanotubes array. Nanoscale Res Lett 5(7):1102–1106. https://doi.org/10.1007/s11671-010-9608-z
18. Yildirimer L, Thanh NTK, Loizidou M, Seifalian AM (2011) Toxicology and clinical potential of nanoparticles. Nano Today 6(6):585–607. https://doi.org/10.1016/j.nanotod.2011.10.001
19. Brown ASC, Hargreaves JSJ (1999) Sulfated metal oxides catalysts. Superactivity through superacidity? Green Chem 1:17–20. https://doi.org/10.1039/A807963C
20. Accorsi G, Listorti A, Yoosaf K, Armaroli N (2009) 1,10-Phenanthrolines: versatile building blocks for luminescent molecules, materials and metal complexes. Chem Soc Rev 38(6):1690. https://doi.org/10.1039/b806408n
21. Abebe A, Atlabachew M, Liyew M, Ferede E (2018) Synthesis of organic salts from 1,10-phenanthroline for biological applications. Cogent Chem 4:1476077. https://doi.org/10.1080/23312009.2018.1476077
22. Hoxha K, Case DAH, Day GM, Prior TJ (2015) Cryst Eng Comm 17:7130–7141. https://doi.org/10.1039/C5CE01286D
23. Sietsma JRA, van Dillen AJ, de Jongh PE, de Jong KP (2006) Application of ordered mesoporous materials as model supports to study catalyst preparation by impregnation and drying, In: Gaigneaux EM, Devillers M, De Vos DE, Hermans S, Jacobs PA, Martens JA, Ruiz P (eds) Studies in Surface and Catalysis, 162, Scientific bases for the preparation of heterogeneous catalysts. Elsevier, Amsterdam, pp. 95–102
24. Istadi I, Anggoro DD, Buchori L, Rahmawati DA, Intaningrum D (2015) Active acid catalyst of sulphated zinc oxide for transesterification of soybean oil with methanol to biodiesel. Proc Environ Sci 23:385–393. https://doi.org/10.1016/j.proenv.2015.01.055
25. Bai Z, Guo Y, Yang L, Li L, Li W, Xu P, Hu C, Wang K (2011) Highly dispersed Pd nanoparticles supported on 1,10-phenanthroline-functionalized multi-walled carbon nanotubes for electrooxidation of formic acid. J Power Sources 196:6232–6237. https://doi.org/10.1016/j.jpowsour.2011.03.020
26. Thakuria R, Nath NK, Saha BK (2019) The nature and applications of π–π interactions: a perspective. Cryst Growth Des 19(2):523–528. https://doi.org/10.1021/acs.cgd.8b01630
27. Yu J, Kim HJ, Go MR, Bae SH, Choi SJ (2017) ZnO interactions with biomatrices: effect of particle size on ZnO-protein Corona. Nanomaterials 7(11):377. https://doi.org/10.3390/nano7110377
28. Auría-Soro C, Nesma T, Juanes-Velasco P, Landeira-Viñuela A, Fidalgo-Gomez H, Acebes-Fernandez V, Gongora R, Almendral Parra MJ, Manzano-Roman R, Fuentes M (2019) Interactions of nanoparticles and biosystems: microenvironment of nanoparticles and biomolecules in nanomedicine. Nanomaterials 9(10):1365. https://doi.org/10.3390/nano9101365
29. Sikora A, Bartczak D, Geißler D, Kestens V, Roebben G, Ramaye Y, Varga Z, Palmai M, Shard AG, Goenaga-Infante H, Minelli C (2015) A systematic comparison of different techniques to determine the zeta potential of silica nanoparticles in biological medium. Anal Methods 7:9835–9843. https://doi.org/10.1039/c5ay02014j
30. Meißner T, Oelschlägel K, Potthoff A (2014) Implications of the stability behavior of zinc oxide nanoparticles for toxicological studies. Int Nano Lett 4:116. https://doi.org/10.1007/s40089-014-0116-5
31. Birnboim HC (1992) Effect of lipophilic chelators on oxyradical-induced DNA strand breaks in human granulocytes: paradoxical effect of 1,10-phenanthroline. Arch Biochem Biophys 294(1):17–21. https://doi.org/10.1016/0003-9861(92)90130-o
32. Wang J, Yu Y, Lu K, Yang M, Li Y, Zhou X, Su Z (2017) Silica nanoparticles induce autophagy dysfunction via lysosomal impairment and inhibition of autophagosome degradation in hepatocytes. Int J Nanomed 12:809–825. https://doi.org/10.2147/IJN.5123596
33. Sizochenko N, Mikolajczyk A, Syzochenko M, Puzyn T, Leszczynski J (2021) Zeta potentials (ζ) of metal oxide nanoparticles: a meta-analysis of experimental data and predictive neural networks modeling. Nanoimpact 22:100317. https://doi.org/10.1016/j.impact.2021.100317
34. Liao C, Jin Y, Li Y, Tjong SC (2020) Interactions of zinc oxide nanostructures with mammalian cells: cytotoxicity and photocatalytic toxicity. Int J Mol Sci 21(17):6305. https://doi.org/10.3390/ijms21176305
35. Boucher D, Denault JB (2012) Caspase family. In: Choi, S (ed) Encyclopedia of signaling molecules. Springer, New York, NY. https://doi.org/10.1007/978-1-4419-0461-4_176
36. Brentnall M, Rodríguez-Menocal L, Ladron d Guevara R, Cepero E, Boise LH (2013) Caspase-9, caspase-3 and caspase-7 have distinct roles during intrinsic apoptosis. BMC Cell Biol 14:32. https://doi.org/10.1186/1471-2121-14-32
37. Wang SW, Lee CH, Lin MS, Chi CW, Chen YJ, Wang GS, Liao KW, Chiu LP, Wu SH, Huang DM, Chen L, Shen YS (2020) ZnO nanoparticles induced caspase-dependent apoptosis in gingival squamous cell carcinoma through mitochondrial dysfunction and p70S6K signaling pathway. Int J Mol Sci 21(5):1612. https://doi.org/10.3390/ijms21051612
38. Li Z, Guo D, Yin X, Ding S, Shen M, Zhang R, Wang Y, Xu R (2020) Zinc oxide nanoparticles induce human multiple myeloma cell death via reactive oxygen species and Cyt-C/Apaf-1/Caspase-9/Caspase-3 signaling pathway in vitro. Biomed Pharmacother 122:109712. https://doi.org/10.1016/j.biopha.2019.109712
39. McLaughlin-Drubin ME, Münger K (2009) The human papillomavirus E7 oncoprotein. Virology 384(2):335–344. https://doi.org/10.1016/j.virol.2008.10.006
40. Mohamed Asik RM, Gowdhami B, Mohamed Jaabir MS, Archunan G, Suganthy N (2019) Anticancer potential of zinc oxide nanoparticles against cervical carcinoma cells synthesized via biogenic route using aqueous extract of Gracilaria edulis. Mat Sci Eng C 103:109840. https://doi.org/10.1016/j.msec.2019.109840
41. Pandurangan M, Enkhtaivan G, Kim DH (2016) Anticancer studies of synthesized ZnO nanoparticles against human cervical carcinoma cells. J Photochem Photobio B Biol 158:206–2011. https://doi.org/10.1016/j.jphotobiol.2016.03.002
42. Rad MM, Najafzadeh N, Tata N, Jafari A (2018) Ag–ZnO nanocomposites cause cytotoxicity and induce cell cycle arrest in human gastric and melanoma cancer cells. Pharm Chem J 52:112–116. https://doi.org/10.1007/s11094-018-1774-9
43. Deegan C, McCann M, Devereux M, Coyle B, Egan DA (2007) In vitro cancer chemotherapeutic activity of 1,10-phenanthroline (phen), $[Ag_2(phen)_3(mal)]x2H_2O$, $[Cu(phen)_2(mal)]x2H_2O$ and $[Mn(phen)_2(mal)]x2H_2O$ ($malH_2$=malonic acid) using human

cancer cells. Cancer Lett 247(2):224–233. https://doi.org/10.1016/j.canlet.2006.04.006

44. Zhang Z, Bi C, Schmitt SM, Fan Y, Dong L, Zuo J, Ping DQ (2021) 1,10-Phenanthroline promotes copper complexes into tumor cells and induces apoptosis by inhibiting the proteasome activity. J Biol Inorg Chem 17(8):1257–1267. https://doi.org/10.1007/s00775-012-0940-x